Journal of Computational Physics 229 (2010) 1897–1908

Contents lists available at ScienceDirect

Journal of Computational Physics

journal homepage: www.elsevier.com/locate/jcp

Application of the RBF meshless method to the solution of the radiative transport equation

Manuel Kindelan *, Francisco Bernal, Pedro González-Rodríguez, Miguel Moscoso

Gregorio Millán Institute, Universidad Carlos III de Madrid, Avenida de la Universidad 30, 28911 Leganés, Spain

ARTICLE INFO

Article history:
Received 25 June 2009
Received in revised form 6 November 2009
Accepted 9 November 2009
Available online 17 November 2009

Keywords:
Radial basis functions
Radiative transfer
Mesh-free

ABSTRACT

In this paper, we introduce a radial basis function collocation method for computing solutions to the time-dependent radiative transfer equation. For these computations, we use finite differences to discretize the time coordinate, a discrete ordinate method to discretize the directional variable, and an expansion in radial basis functions to approximate the spatial dependence of the solution. The main advantages of the RBF method are that it does not require any mesh or grid, achieves spectral accuracy in multi-dimensions for arbitrary node layouts, and it is extremely simple to implement.

1. Introduction

The equation of radiative transfer is an integral-partial differential equation widely used in different research areas to model wave motions such as light propagation through a turbulent atmosphere [8,31], electromagnetic waves propagating in plasmas [56,61], or seismic wave propagation [52,53,1]. Similar type of equations govern particle motions in applications such as neutron transport in a reactor [7,43] or electron transport in radiation therapy [58]. Lately, it is also attracting a lot of attention in the context of light propagation in biological tissue due to its applications to optical imaging [10,39,37].

Although it is a very well known equation, analytical solutions are only available for the simplest problems [8,7]. Therefore, numerical solutions are needed in practical situations. However, it is computationally very demanding and several challenges arise when solving it numerically. The main one is caused by its large dimensionality (one time variable, two directional variables, and three spatial variables). In addition, in many applications the medium scatters with a sharp peak in the forward direction and one must resolve the directional dependence carefully. Furthermore, the dependent variable can be discontinuous with respect to direction due to the boundary conditions and the presence of sharp interfaces in the medium.

One possibility is to solve the radiative transport equation using Monte Carlo methods (see [49] and references therein). These methods simulate the trajectories of particles mimicking the random walk of the physical particle transport process. Other than Monte Carlo simulations, direct numerical methods such as finite differences [43,39] and finite elements [58,57] have been applied to spatial discretizations of the transport equation. The convergence rate of finite element schemes are superior to the usual diamond scheme employed in finite differences schemes. Also, the discontinuous Galerkin method has been applied to discretize the spatial variable [60,24] and capture the possible sharp gradients and near discontinuities of the solution close to material interfaces.

* Corresponding author. Fax: +34 91 624 91 29.
E-mail addresses: kinde@ing.uc3m.es (M. Kindelan), fcoberna@math.uc3m.es (F. Bernal), pgonzale@math.uc3m.es (P. González-Rodríguez), moscoso@math.uc3m.es (M. Moscoso).

0021-9991/$ - see front matter © 2009 Elsevier Inc. All rights reserved.
doi:10.1016/j.jcp.2009.11.014

Mesh-free or *element free* methods have arisen considerable interest because they eliminate the labor intensive step of mesh generation inherent to finite element methods. On the one hand, meshless methods eliminate the need of element connectivity in the solution of partial differential equations. On the other hand, they do not require regularly spaced nodes, so they also offer an advantage over Fourier [51,2] and Chebyshev [35,36] classical spectral techniques.

In this paper we address the solution of the spatial dependence of the equation of radiative transport using the Radial Basis Function (RBF) method. This method has been successfully applied to a large variety of problems to solve linear [15,16,29,30,42,59,17,22] and non-linear [12,5] partial differential equations. However, despite the increasing popularity of radial basis functions, there is not, to our best knowledge, any attempt to use this alternative formulation to spatial discretizations of the radiative transport equation. The aim of this work is to introduce this new methodology to the resolution of the widely applied time-dependent scalar radiative transport equation showing the underlying ideas and its main characteristics. We (i) analyze the performance of radial basis functions, (ii) show their ease of implementation, (iii) study their spectral convergence, and (iv) illustrate their flexibility to handle problems in complicated geometries.

The RBF method was first proposed by Hardy [27] for the purpose of interpolating multi-dimensional surfaces, but it is only in the last 15 years (since the seminal work of Kansa [32,33]) that it has been applied to solving partial differential equations. Kansa's method looks for an approximate solution in the function space spanned by a finite set of Radial Basis Functions, by using collocation of the PDE in a set of (scattered) centers.

Of special interest are infinitely differentiable RBFs, such as the multiquadric. These functions depend on a shape parameter, c, and there is much experimental evidence that the RBF collocation method exhibits spectral $h-c$ convergence. The error decreases exponentially with decreasing h (average distance between RBF centers), and with increasing shape factor c (flat RBFs).

However, the flat basis function limit $(c \to \infty)$ is severely ill-conditioned, since all the basis functions then become approximately constant, and thus linearly dependent. In fact, there is a trade-off between accuracy and ill-conditioning which Schaback explains by a kind of *uncertainty relation* [62,54] which says that the attainable error and the condition number of the RBF interpolation matrix cannot both be small at the same time. It should be mentioned, however, that during the last years, there have been several promising efforts [11,40,19,20,41,21,22] trying to overcome this ill-conditioning difficulty, by making the flat basis function range fully available for computation.

The second main concern regarding RBF methods is its high computational cost, mainly due to the solution of a large and full linear system of equations to derive the coordinates of the solution in the RBFs function space. However, viable approaches have also been proposed [34,3,4] to overcome these difficulties.

Finally, we remind that in order to solve the radiative transport equation on a computational mesh, it must be discretized also in direction to treat the integral operator. In this paper, we have chosen the popular discrete ordinate method [43] to approximate the angular dependence of the solution. We mention, though, that any other choice for the angular discretization, such as spherical harmonic expansions [7], wavelets [26], or finite elements [38,24], would work without interfering with the rest of the algorithm.

The remainder of the paper is as follows: we start describing the equation and boundary conditions for the radiative transport equation. Section 3 describes the numerical scheme to solve the temporal, directional and spatial dependence of the equation. Particular emphasis is paid to the spatial dependence which is solved using the RBF method. Then we describe the results obtained in four different numerical experiments and state the conclusions of this work.

2. Formulation

Wave propagation in a random medium $\mathcal{D} \subset \mathbb{R}^n$ $(n = 2, 3)$ that scatters and absorbs radiation is described by the radiative transport equation

$$v^{-1}\partial_t I(\mathbf{r}, \widehat{\Omega}, t) + \widehat{\Omega} \cdot \nabla_{\mathbf{r}} I(\mathbf{r}, \widehat{\Omega}, t) - \mathcal{L}[I](\mathbf{r}, \widehat{\Omega}, t) = Q(\mathbf{r}, \widehat{\Omega}, t), \tag{1}$$

where I represents the energy density, or intensity, at each position $\mathbf{r}$, unit direction $\widehat{\Omega}$ and time t. In (1), v is the constant wave speed, Q accounts for any sources within the medium $\mathcal{D}$, and the scattering operator $\mathcal{L}$ is defined as

$$\mathcal{L}[I](\mathbf{r}, \widehat{\Omega}, t) = -\mu_t(\mathbf{r}) I(\mathbf{r}, \widehat{\Omega}, t) + \mu_s(\mathbf{r}) \int_{\mathbb{S}^{n-1}} f(\widehat{\Omega}, \widehat{\Omega}') I(\mathbf{r}, \widehat{\Omega}', t) d\widehat{\Omega}', \tag{2}$$

where the total scattering coefficient $\mu_t = \mu_s + \mu_a$ is the sum of the scattering coefficient μ_s and the absorption coefficient μ_a, and $\mathbb{S}^{n-1}$ denotes the unit circle in 2D problems $(n = 2)$ and the unit sphere in 3D problems $(n = 3)$. The scattering phase function f, which we assume is position independent, gives the fraction of energy in direction $\widehat{\Omega}'$ converted to wave energy in direction $\widehat{\Omega}$, and it is normalized according to

$$\int_{\mathbb{S}^{n-1}} f(\widehat{\Omega}, \widehat{\Omega}') d\widehat{\Omega}' = 1. \tag{3}$$

In biological applications, tissues typically scatter light energy in the forward direction and, therefore, the phase function has a sharp peak at directions $\widehat{\Omega}' \sim \widehat{\Omega}$.

Eq. (1) has to be solved with appropriate initial and boundary conditions. If no radiation other than the source Q enters into the medium, then the boundary condition is

$$I(\mathbf{r},\widehat{\Omega},t)=0, \tag{4}$$

on $\Gamma=\{(\mathbf{r},\widehat{\Omega},t)\in\partial\mathcal{D}\times\mathbb{S}^{n-1}\times[0,T] \text{ s.t. } v(\mathbf{r})\cdot\widehat{\Omega}<0\}$, where $v(\mathbf{r})$ denotes the unit outward normal vector to the boundary $\partial\mathcal{D}$. In addition, we assume that no energy is present in the medium at time $t=0$, and therefore

$$I(\mathbf{r},\widehat{\Omega},0)=0 \quad \text{in } \mathcal{D}\times\mathbb{S}^{n-1}. \tag{5}$$

The transport problem (1)–(5) is well-posed [7].

3. Numerical scheme

The numerical solution of the time-dependent radiative transfer equation requires discretization of spatial, angular and temporal domains. Therefore, three numerical treatments make up our numerical scheme in total. First, we use finite differences to discretize the time coordinate. Then, we use a discrete ordinate method and a quadrature rule to approximate the integral operator. Finally, for each time and direction, we compute a continuous solution in the functional space spanned by a finite set of Radial Basis Functions (RBF's).

For the ease of presentation we consider here wave propagation in a 2D homogeneous medium. In this case, the radiative transfer equation reads

$$v^{-1}\partial_t I(\mathbf{r},\theta,t)+\cos\theta\,\partial_x I(\mathbf{r},\theta,t)+\sin\theta\,\partial_y I(\mathbf{r},\theta,t)-\mathcal{L}[I](\mathbf{r},\theta,t)=Q(\mathbf{r},\theta,t), \tag{6}$$

on $\mathcal{D}\times[0,2\pi]\times[0,T]$, with the corresponding 2D boundary and initial conditions. In Eq. (6), θ represents the angle corresponding to direction $\widehat{\Omega}$.

3.1. Temporal discretization

To discretize (6), we use a second order, backward difference approximation. Hence, defining $I_i=I(\mathbf{r},\theta,t_i)$ as the intensity at the coordinate time $t_i=i\Delta t, i=1,2,\ldots,K$, Eq. (6) can be written as

$$\cos\theta\,\partial_x I_i+\sin\theta\,\partial_y I_i+\left(\mu_t+\frac{3}{2v\Delta t}\right)I_i=J_i, \tag{7}$$

where an apparent source term at time t_i has been defined as

$$J_i=Q_i+\mu_s\int_{S^{n-1}}f(\theta,\theta')I_i(\theta')d\widehat{\Omega}'+\frac{2I_{i-1}}{v\Delta t}-\frac{I_{i-2}}{2v\Delta t}, \tag{8}$$

to include the source term, the scattering source term, and the contribution of the time derivative term.

To describe scattering, we use the Henyey–Greenstein phase function, which in two dimensions is [28]

$$f(\theta,\theta')=\frac{1}{2\pi}\frac{1-g^2}{1+g^2-2g\cos(\theta-\theta')}, \tag{9}$$

where g is the mean cosine scattering angle or anisotropy factor. Scattering is isotropic for $g=0$, and becomes more and more sharply peaked in the forward direction as $g\to 1$.

3.2. Directional discretization

In order to numerically solve the directional dependence of the solution, we choose a discrete ordinate method because of its ease of implementation and good accuracy. Hence, we solve (7) along particular directions and use a quadrature rule to approximate the integral operator. In other words, we select a set of directions $\theta_m, m=1,\ldots,M$, together with appropriate weight factors $w_{mm'}, m,m'=1,\ldots,M$, and write (8) as

$$J_i=Q_i+\mu_s\sum_{m'=1}^{M}w_{mm'}I(\mathbf{r},\theta_{m'},t_i)+\frac{2I_{i-1}}{v\Delta t}-\frac{I_{i-2}}{2v\Delta t}. \tag{10}$$

Here, we have considered M discrete directions defined as $\theta_m=(m-1)\Delta\theta$ with $\Delta\theta=2\pi/M$, and the weights have been chosen to be [9,25]

$$w_{mm'}=\int_{\theta_{m'}-\Delta\theta/2}^{\theta_{m'}-\Delta\theta/2}f(\theta_m,\theta')d\theta', \tag{11}$$

with the property

$$\sum_{m'=1}^{M} w_{mm'} \approx 1 \quad \text{for all } m. \tag{12}$$

Using this discretization, we obtain a set of partial differential equations in space. Note that the resultant system of equations is coupled in directions, leading to very large matrices to invert. A convenient way to circumvent this problem and solve this system of equations efficiently is to use the source iteration method [44]. In this method, the intensity in the integral operator is assumed to be known from previous iterations. Thus, using the superscript l as iteration number, and denoting by $I_{mi} = I(\mathbf{r}, \theta_m, t_i)$ the continuous solution in space at discrete direction and time coordinates θ_m and t_i, respectively, the equations to be solved are

$$\cos\theta_m \partial_x I^l_{mi} + \sin\theta_m \partial_y I^l_{mi} + \left(\mu_t + \frac{3}{2v\Delta t}\right) I^l_{mi} = J^{l-1}_{mi} \tag{13}$$

with

$$\begin{aligned} J^0_{mi} &= Q_{mi} + \frac{2I_{m,i-1}}{v\Delta t} - \frac{I_{m,i-2}}{2v\Delta t}, \quad \text{and} \\ J^l_{mi} &= Q_{mi} + \mu_s \sum_{m'=1}^{M} w_{mm'} I^l_{m'i} + \frac{2I_{m,i-1}}{v\Delta t} - \frac{I_{m,i-2}}{2v\Delta t}, \quad l = 1, 2, \ldots \end{aligned} \tag{14}$$

Eq. (13) is solved iteratively until convergence,

$$\| I^l_{mi} - I^{l-1}_{mi} \| < \epsilon, \tag{15}$$

where ϵ is a user defined termination parameter.

Numerical solution of (13) and (14) involves updating the source term J^{l-1}_{mi} by numerical quadrature of the scattering operator, and numerical solution of the hyperbolic partial differential Eq. (13) for each discrete direction θ_m. Note that with this method, each direction is independent from the others, and consequently, the computational cost increases only linearly with respect to the number of directions used in the numerical scheme (certainly, at the price of iterating).

3.3. Spatial discretization

Finally, for the numerical solution of Eq. (13) in each direction, we use the RBF collocation method, also known as Kansa's method [32,33].

With Kansa's method we look for an approximate solution of the problem in the functional space spanned by shifted smooth functions whose argument is the distance to a set of N RBF centers. Thus, for each direction θ_m,

$$I^l_{mi}(\mathbf{r}) = \sum_{j=1}^{N} \alpha_j(\theta_m, t_i) \phi_j(\|\mathbf{r} - \mathbf{r}_i\|), \tag{16}$$

where $\mathbf{r}_j = (x_j, y_j), j = 1, \ldots, N$, is the set of RBF centers, and $\|\cdot\|$ represents the usual l_2 norm. In this work, we use the multiquadric as RBF function,

$$\phi_j(x, y) = \sqrt{(x - x_j)^2 + (y - y_j)^2 + c^2}, \quad j = 1 \ldots N, \tag{17}$$

where c is the shape parameter. The multiquadric was originally proposed by Hardy [27] for interpolation of scattered data, and has been used extensively both for interpolation and for the solution of PDEs. In a thorough study of interpolation methods for 2D scattered data, Franke [23] found that the multiquadric generally performs best. In fact, it has been shown that multiquadrics has exponential convergence for approximation of functions [46,47,62]. Also, it was shown by Driscoll and Fornberg [11] that, in 1D, in the limit $c \to \infty$ (flat RBFs) the RBF method reproduces pseudospectral methods if the nodes are placed accordingly (i.e. equispaced nodes for Fourier methods, Gauss-Chebyshev nodes for Chebyshev methods, etc.).

The coefficients $\{\alpha_j\}$ in (16) are determined by collocation. Since there are $N \times M$ coefficients for each time t_i, we need $N \times M$ collocation equations. In this work we use the same set of N RBF centers as collocation nodes. Thus, at each interior node, collocation of Eq. (13) leads to

$$\sum_{j=1}^{N} \alpha_j(\theta_m, t_i) \left[\cos\theta_m \frac{\partial \phi_{jk}}{\partial x} + \sin\theta_m \frac{\partial \phi_{jk}}{\partial y} + \left(\mu_t + \frac{3}{2v\Delta t}\right) \phi_{jk} \right] = J^{l-1}_{mi}, \quad k = 1, 2, \ldots, N - N_B, \tag{18}$$

where $\phi_{jk} = \phi_j(x_k, y_k)$, and N_B is the number of boundary nodes with ingoing direction.

At each boundary node, we either use Eq. (18) for outward going directions $v(\mathbf{r}_j) \cdot \widehat{\Omega} > 0$, or collocation of the boundary condition (4) for ingoing directions $v(\mathbf{r}_j) \cdot \widehat{\Omega} < 0$, in which case

$$\sum_{j=1}^{N} \alpha_j(\theta_m, t_i) \phi_{jk} = 0, \quad k = N - N_B + 1, N - N_B + 2, \ldots, N. \tag{19}$$

Thus, at each time step t_i, and each iteration l, M independent linear systems of N equations with N unknowns have to be solved to derive the $N \times M$ coefficients α_j. Notice however, that the matrix of the linear system for each direction θ_m, does not vary neither with iteration nor with time step and, therefore, factorization of the resulting matrices has to be carried out only once. Thus, using the *LU* factorization method, the computational cost is $(2/3)N^3M$ flops resulting from factorization, plus, $2N^2KMN_{iter}$ flops resulting from solution of the resulting triangular systems (N_{iter} is the number of iterations needed to satisfy the convergence criterion (15), and K the number of time steps). Notice that the most computationally expensive part of the algorithm (*LU* factorization) is fully parallelizable, since each direction can be solved independently of the other directions. The only step which has to be carried out sequentially is the computation of the scattering term. To our knowledge there are not theoretical results regarding the invertibility of the linear system associated to collocation of PDEs using an arbitrary set of RBF centers [13]. In practice, however, for this and other PDE problems we have never found singular matrices.

If instead of using RBFs in the two dimensional space (x, y), we had used RBF's in the two plus one dimensional space of locations and directions (x, y, θ), a linear system of $N \times M$ equations with $N \times M$ unknowns would have to be solved. Thus, the computational cost of the factorization would have been $(2/3)N^3M^3$. The ratio of computational cost with respect to the proposed method is thus M^2.

4. Numerical experiments

To evaluate our numerical method, we present in this section computations for different radiative transfer problems. In this computations we normalize spatial units by $l = 1/\mu_t^{(0)}$, and time units by l/v, where $\mu_t^{(0)}$ is the total scattering coefficient of the background medium. To examine the results we compute the total intensity $\mathcal{I}_{tot}$ and the flux $\mathcal{F}$, defined as

$$\mathcal{I}_{tot}(\mathbf{r}, t) = \sum_{i=0}^{M} I(\mathbf{r}, \theta_i, t), \quad \text{and} \quad \mathcal{F}(\mathbf{r}, t) = \sum_{i=0}^{M} I(\mathbf{r}, \theta_i, t)|\cos\theta_i|,$$

respectively, in addition to the intensity I at each direction. The choice of the discretization parameters is highly problem dependent and should be a trade-off between accuracy and cost. In the following examples we have used $M = 64$ discrete directions to accurately resolve the peak of the scattering function.

4.1. Problem 1

To assess the accuracy and the consistency of the proposed meshless method, we first consider the following homogeneous and steady problem in a square $\Omega \equiv [-10, 10] \times [-10, 10]$. For this simple example, the source is

$$Q(x, y, \theta) = \mu_a e^{-4\mu_a(x^2+y^2)}(1 - 8x\cos\theta - 8y\sin\theta),$$

and the boundary condition is

$$I(x_b, y_b, \theta) = e^{-4\mu_a\left(x_b^2+y_b^2\right)},$$

on $\Gamma_{in} = \{\partial\Omega \times [0, 2\pi] \text{ s.t.} \mathbf{n}(x_b, y_b) \cdot \hat{\boldsymbol{\theta}} < 0\}$. The parameters of the medium are $\mu_s = 1mm^{-1}, \mu_a = 0.01mm^{-1}, g = 0.9$. This (artificial) problem has the following exact isotropic solution,

$$I_e(x, y, \theta) = e^{-4\mu_a(x^2+y^2)} \quad \text{for all } \theta \in [0, 2\pi].$$

To solve this problem, we use a set of RBF centers located on an equally spaced grid of $N = N_x \times N_y$ nodes. For simplicity, we use the same set of points as collocation nodes. Thus, for each direction we use collocation of the boundary condition, so that

$$\sum_{j=1}^{N} \alpha_j(\theta)\phi_{jb} = e^{-4\mu_a(x_b^2+y_b^2)},$$

on a subset of N_b boundary nodes of ingoing directions ($N_b \leqslant N_x + N_y$), and Eq. (18) on the remaining $N - N_b$ collocation nodes. The resulting M linear systems of N^2 equations with N^2 unknowns are solved by *LU* factorization.

The following quantities are used to measure the difference between the analytical solution I_e, and the numerical solution I:

$$\epsilon_{max} = \max_{ij} |I(\theta_i, x_j, y_j) - I_e(\theta_i, x_j, y_j)|, \tag{20}$$

$$\epsilon_{mse} = \frac{1}{N_\theta N_f} \sum_{i=1}^{N_\theta} \sum_{j=1}^{N_f} (I(\theta_i, x_j, y_j) - I_e(\theta_i, x_j, y_j))^2, \tag{21}$$

where (x_j, y_j) are a set of evaluation nodes on an equally spaced grid of $N_f = 51 \times 51$ nodes.

The left part of Fig. 1 shows the maximum error ϵ_{max} as a function of the shape parameter c using four different resolutions $N = 11 \times 11, 21 \times 21, 31 \times 31$, and 41×41. The right part shows the corresponding dependence of the mean squared

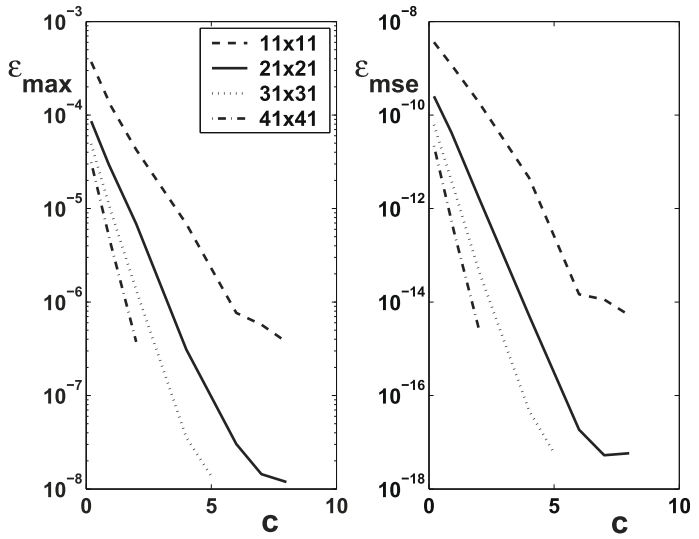

Fig. 1. Left: maximum error as a function of the shape parameter for $M = 64$, and for spatial resolutions $N = 11 \times 11$ (dashed line), $N = 21 \times 21$ (solid line), $N = 31 \times 31$ (dotted line), and $N = 41 \times 41$ (dot-dashed line). Right: mean squared error as a function of shape parameter.

error ϵ_{mse}. The usual exponential convergence of the RBF method with respect to shape parameter can be clearly observed. Notice the high accuracy of the method, resulting in maximum errors of the order of 10^{-8}, and mean squared errors of the order of 10^{-17} with a relatively coarse grid of 21×21 nodes We note that for each resolution there is an optimal value of c such that, for higher values the resulting linear system becomes too ill-conditioned, and round-off errors deteriorate the accuracy of the solution.

These results show the accuracy and convergence properties of the proposed method. However, it is a non-physical problem (negative sources, non-zero incoming light intensity, isotropic solution,...) that hides some of the main difficulties of the numerical solution of the radiative transport equation. For instance, since the solution is isotropic in angle space, computation of the scattering term by numerical integration is exact, and only errors due to the space dependence of the solution are observed. Typical solutions of the radiative transport equation exhibit discontinuities with respect to direction which do not appear in this artificial problem. The following problem includes these difficulties.

4.2. Problem 2

As a second problem we solve the following non-isotropic, steady problem, in a square $\Omega \equiv [-1.5, 1.5] \times [-1.5, 1.5]$. The boundary condition is

$$I(x_b, y_b, \theta) = 0 \quad \text{on } \Gamma_{in} = \{\partial\Omega \times [0, 2\pi] \text{ s.t. } \mathbf{n}(x_b, y_b) \cdot \hat{\boldsymbol{\theta}} < 0\},$$

and the source is given by

$$Q(x, y, \theta) = \frac{2}{\pi} e^{-2(x^2+y^2)}.$$

The parameters of the (homogeneous) medium are $\mu_s = 1 mm^{-1}$, $\mu_a = 0 mm^{-1}$ and $g = 0.9$.

The left side of Fig. 2 shows the intensity distribution in direction $\theta_i = \pi, I(x, y, \pi)$, and the right side shows the total intensity, $\mathcal{I}_{tot}(x, y)$, obtained using a set of $N = 121$ RBF centers located on a rectangular equispaced grid of 11×11 nodes, $M = 64$ angular directions, and shape parameter $c = 2$. The solution is computed on an equally spaced fine grid of $N_f = 51 \times 51$ nodes.

This problem does not have an analytical solution and, therefore, to assess the accuracy of the proposed method, it is not possible to use the error of the numerical solution, as it was done in the previous problem. In this case, we will use the residual in a fine equispaced grid, defined as,

$$R(x_k, y_k, \theta_i) = \sum_{j=1}^{N} \alpha_j(\theta_i) \left[\cos\theta_i \frac{\partial \phi_{jk}}{\partial x} + \sin\theta_i \frac{\partial \phi_{jk}}{\partial y} + \mu_a \phi_{jk} \right] - \mu_s \mathcal{L}[I] - Q.$$

Fig. 3 shows the maximum residual R_{max}, and the mean squared residual R_{mse} as a function of the shape parameter c (R_{max} and R_{mse} are defined as in (20) and (21) with R instead of $I - I_e$). As in the previous problem, exponential convergence with respect to the shape parameter can be clearly observed. Also notice that the rate of convergence increases with the number of RBF

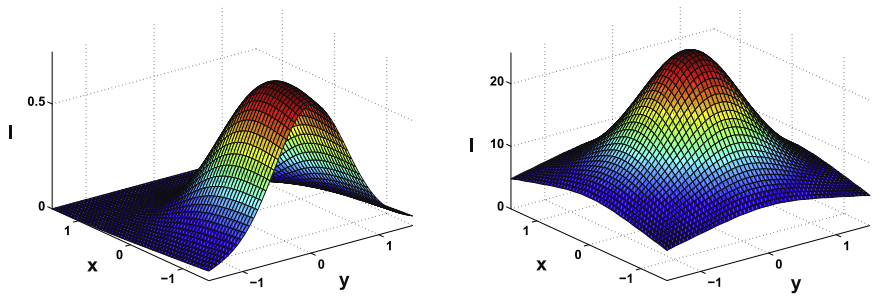

Fig. 2. RBF solution of problem 2. $N = 121, M = 64, c = 2$. Left: light intensity distribution in direction $\theta = \pi$. Right: total light intensity distribution.

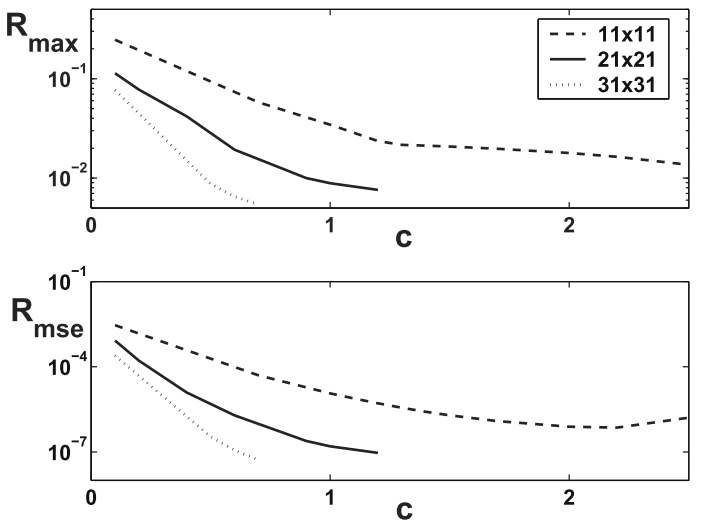

Fig. 3. Top: maximum residual as a function of the shape parameter ($M = 64$). Bottom: mean squared residual as a function of shape parameter ($M = 64$).

centers. Again, for each number of RBF centers, there is a critical value of c above which the resulting linear system becomes too ill-conditioned, and round-off error deteriorates the accuracy of the solution.

It is interesting to check the residual distribution on a fine grid. The left side of Fig. 4 shows the residual distribution for direction $\theta_i = \pi$, using $N = 121$ collocation points, $M = 64$ directions, and $c = 1.7$ as shape parameter (this residual distribution corresponds to the intensity distribution shown on the left side of Fig. 2). Notice that the residual is quite low throughout the domain, except near the boundary at $x = 1.5$ where the residuals are rather high. In fact, for $\theta_i = \pi, x = 1.5$ is the only inward going boundary where collocation of the boundary condition (19), instead of collocation of Eq. (18), is enforced. Thus,

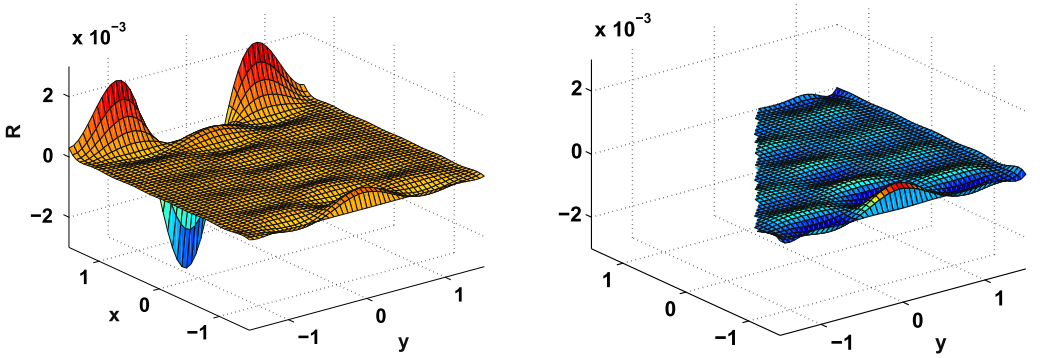

it should be expected that the residuals, and therefore also the errors, are higher near the boundary in which the residual is not forced to be zero. Similar behavior can be observed for any other direction; residuals and errors are higher near the boundaries where the boundary condition is enforced.

Inaccuracies near the boundaries is a well known drawback of the RBF method [18]. One way to improve the accuracy of the method was first proposed by Fedoseyev et al. [14] and later used by many authors [50,63,5]. It is based on enforcing collocation of the PDE also at the boundary nodes. Thus, we enforce collocation of the PDE in all nodes, including ingoing boundary nodes $(N - N_B + 1, \ldots, N)$. Therefore, Eq. (19) is enforced in N nodes, and Eq. (4) is enforced in N_B nodes, leading to a system of $N + N_B$ equations with N unknowns which is solved in a least square sense, by computing the pseudoinverse through the *Singular Value Decomposition (SVD)*. The right side of Fig. 4 shows the resulting residual distribution. Notice that the residual peak near the boundary at $x = 1.5$ has now disappeared. In fact, the maximum residual (for all nodes in the fine grid and for all directions) has decreased from $R_{max} = 1.97 \times 10^{-2}$ to $R_{max} = 4.71 \times 10^{-3}$, and the mean squared residual from $R_{mse} = 1.22 \times 10^{-6}$ to $R_{mse} = 1.55 \times 10^{-7}$.

4.3. Problem 3

As a third numerical experiment we solve the following unsteady problem in a non-homogeneous medium. A normally incident $(\theta = 0)$ beam of spatial width $w_s = 1/\sqrt{10}$ impinges upon a rectangular medium $\Omega \equiv [-2.5, 2.5] \times [-2.5, 2.5]$ at the location $(x_s, y_s) = (-2.5, 1.5)$. We incorporate, this beam into our formulation through the boundary condition

$$I(x = -2.5, y, \theta, t) = f(t) \exp\left[-\left(\frac{y - y_s}{w_s}\right)^2\right] \delta(\theta - 0), \tag{22}$$

for $0 \leqslant \theta < 2\pi$ and $t \in [0, T]$. In (22),

$$f(t) = \frac{2}{\pi} \exp\left[-\left(\frac{t - t_o}{w_t}\right)^2\right] \tag{23}$$

is the temporal pulse shape of width $w_t = 1/\sqrt{2}$. The time at which the pulse center reaches the boundary is t_o. This is the only source of radiation. Accordingly, $Q = 0$ in (1), and we impose homogeneous boundary conditions on the other edges of the domain, i.e., $I(x = 2.5, y, \theta, t) = I(x, y = -2.5, \theta, t) = I(x, y = 2.5, \theta, t) = 0$ for all $\theta \in [0, 2\pi]$ and $t \in [0, T]$.

The scattering coefficient is equal to 1 mm^{-1} throughout the domain, except in the interior of a circle of radius 0.3 centered at (1,1.5), where the scattering coefficient is equal to 5 mm^{-1}. Thus,

$$\mu_s = \begin{cases} 1 \text{ mm}^{-1} & \text{if } \sqrt{(x-1)^2 + (y-1.5)^2} > 0.3 \\ 5 \text{ mm}^{-1} & \text{if } \sqrt{(x-1)^2 + (y-1.5)^2} \leqslant 0.3 \end{cases}.$$

The other parameters are constant and equal to $\mu_a = 0.01$ mm^{-1}, $g = 0.7$, $\nu = 1$.

Fig. 5 shows the numerical solution of this problem obtained with $N = 961$ RBF centers and collocation points, $M = 64$ directions, shape parameter $c = 0.3$, and time step $dt = 0.1$. The total intensity $\mathcal{I}_{tot}(x, y, t_i)$ in the domain is shown at times $t_i = 2$ (top left image), $t_i = 4$ (top right image), and $t_i = 6$ (bottom left image). Notice, that for time $t_i = 6$, the signal has arrived to the small obstacle of higher scattering coefficient, resulting in lower energy density in that region.

In the bottom right image of Fig. 5 we show, in solid line, the backscattered flux $\mathcal{F}(x_b, y_b, t)$ measured at location $(x_b, y_b) = (-2.5, -0.5)$. Notice, that the scattering obstacle generates a bump in the backscattered response starting around $t = 7$. In fact, the pulse takes 3.2 time units to travel from the source located at $(-2.5, 1.5)$ to the scatterer edge at $(0.7, 1.5)$, and around 3.8 time units to travel back to the measurement location at $(-2.5, -0.5)$. For comparison purposes, we have plotted in dashed line the backscattered flux response for the case of a homogeneous medium in which the scattering obstacle is not present.

4.4. Problem 4

As a last numerical experiment we solve the following non-homogeneous, steady problem in a circular domain of radius $r = \sqrt{2}$, centered at (0,0). Therefore, $\Omega = \{(x, y) \text{ s.t. } r \equiv \sqrt{x^2 + y^2} \leqslant \sqrt{2}\}$. A normally incident beam $(\theta = 0)$ illuminates the medium at $\left(-\sqrt{2}, 0\right)$. This is the only source, which is incorporate into the mathematical formulation through the corresponding boundary condition as in the previous problem. Therefore, $Q = 0$ in (1), and

$$I(x, y, \theta) = \frac{2}{\pi} \exp\left[-2\left((x + \sqrt{2})^2 + y^2\right)\right] \delta(\theta - 0),$$

on $\Gamma_{in} = \{\partial\Omega \times [0, 2\pi] \text{ s.t. } \mathbf{n}(x, y) \cdot \hat{\mathbf{s}} < 0\}$.

The scattering coefficient μ_s is equal to 1 mm^{-1} throughout the domain except in the interior of a thin layer near the surface, where the scattering coefficient is very small. Also the absorption coefficient is small in that region. Thus, the scattering and absorption coefficients are

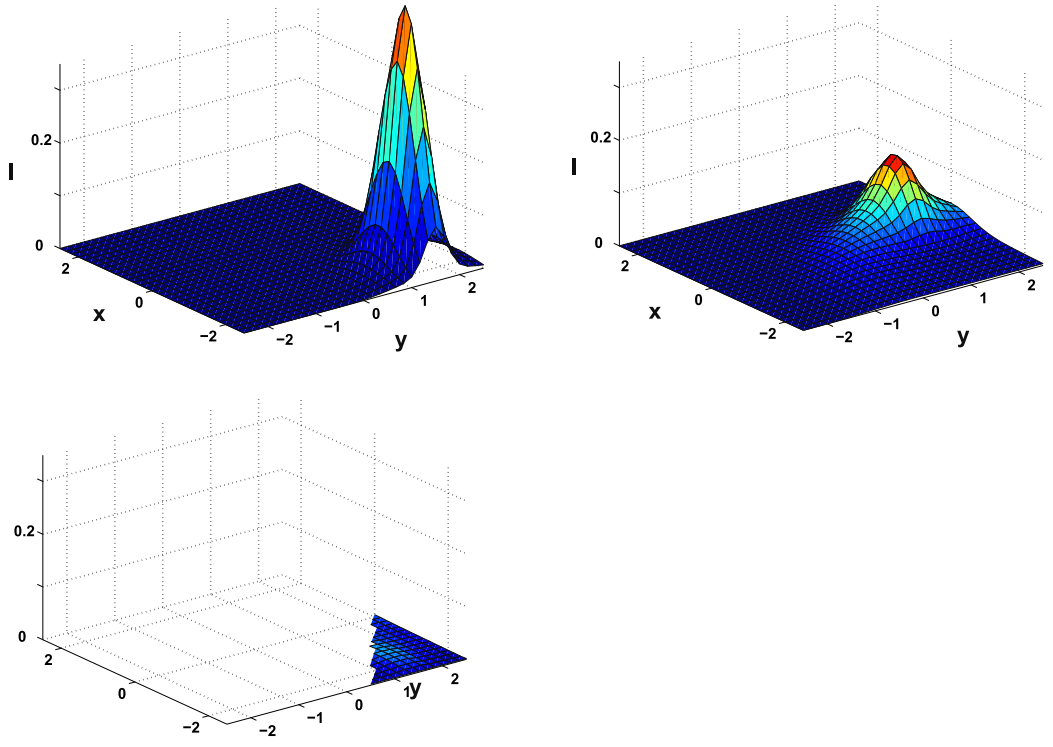

$$\mu_s = 1 - 0.95e^{-80(r-1.1)^2} \quad \text{and} \quad \mu_a = 0.01 - 0.0095e^{-80(r-1.1)^2},$$

respectively. The anisotropy factor is $g = 0.7$.

The top left side of Fig. 6 shows the RBF centers ($*$) and the collocation nodes (o) used in the numerical solution of this problem. In the interior of the domain we use the same RBF centers and collocation nodes. We take advantage of the fact that, with the RBF method, it is very easy to increase the density of nodes in regions where the errors or the residuals are large. In this problem, we expect the errors to be larger in the region near the boundary of the domain, where the source is located and where a sharp change in the scattering and absorption coefficients takes place (shown with dashed red lines in the figure).[1] Therefore, we use a smaller concentration of nodes near the center of the circle and a higher concentration for $r \geqslant 1$. Notice also, that there are some RBF centers located outside of the circle. For each one of these centers we define a new collocation point located at the intersection of the boundary with the line joining the RBF center with the origin. We have used a total of $N = 677$ RBF centers, the same number of collocation nodes, 116 boundary nodes (the same number of RBF centers outside the domain) and $M = 64$ directions.

As mentioned previously, the accuracy of the solution strongly depends on the shape parameter c. As the shape parameter increases, accuracy increases, but the condition number of the resulting linear system also increases. Too large or too small shape parameters make the multiquadric basis too flat or too peaked, and both should be avoided. Thus, an appropriate selection of the shape parameters is crucial. Although there are no definite rules for finding the optimal value, there is general agreement that this is related to the internode distance. Since in this problem the RBF centers are not equally spaced, it is necessary to use a non-constant shape parameter. Thus, in Eq. (17), the shape parameter c should be replaced by c_j. Moody suggested in [48] a non-constant shape parameters $c_i = \lambda d_i$, where d_i is the distance from each RBF center to its nearest neighbour, and λ is a constant factor. In this work we have used $c_j = 0.18$ for RBF centers located in the central region ($r < 1$), and $c_j = 0.005$ for RBF centers located near the boundary ($r \geqslant 1$). These values provide good convergence and small residuals.

The top right side of Fig. 6 shows the intensity I for $\theta = 0$. As with problems 1 and 2, the solution is computed on an equally spaced fine grid of $N_f = 51 \times 51$ nodes. The intensity is maximum at the source $\left(-\sqrt{2}, 0\right)$ and decreases throughout the domain. Notice that in the annular region of small scattering and absorption, the intensity is approximately constant. The

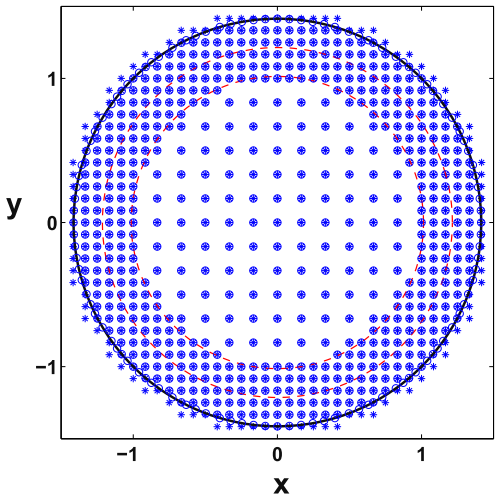

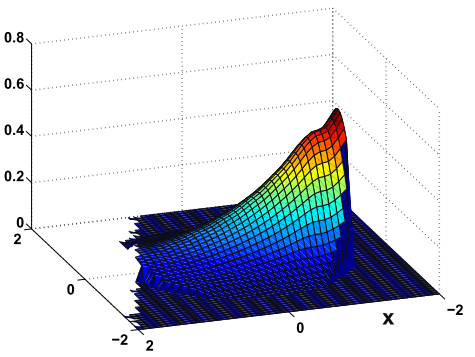

bottom left side of Fig. 6 shows the intensity for $\theta = \pi/2$. In this case, the maximum value is 0.0036 and takes place at approximately $(-1,0)$. The bottom right side of Fig. 6 shows the total energy distribution $\mathcal{I}_{tot}$. Notice that, as was the case for $\theta = 0, \mathcal{I}_{tot}$ is maximum at the source location, and almost constant in the region with low scattering and absorption coefficients. However, far from the source the total intensity is much higher than the intensity at $\theta = 0$ due to the contribution of scattering in all directions.

5. Conclusions

This paper is an initial effort towards developing an RBF meshless method for the radiative transport equation. In particular, we have analyzed the effectiveness and performance of the RBF methodology to numerically solve the spatial dependence of the radiative transport equation. Using a set of numerical experiments, we have corroborated that the well known advantages of the method also apply to the solution of the radiative transport equation, namely,

- Ease of implementation; in all test cases the code is short and simple.
- Spectral accuracy; a small number of nodes provides highly accurate results.
- Fully meshless; the expensive task of generating a computational mesh over an irregular domain is replaced by the much easier task of scattering nodes.
- Domain flexibility; well suited for the solution of problems in irregularly shaped domains.
- Easily extended to 3D; algorithmic complexity does not increase with dimension since RBFs only depend on a scalar (the Euclidean distance between nodes).
- Opportunities for combining spectral accuracy with local refinement.

We consider that these advantages illustrate that the RBF methodology can be a promising new approach for the numerical solution of the radiative transport equation. However, there are two main concerns that may hamper its acceptance; computational cost and stability.

The high computational cost of the method is mainly due to the need to solve large and full linear system of equations to derive the coordinates of the solution in the RBFs function space. In the method that we propose for the radiative transport equation, this concern is alleviated by the fact that factorization of the matrix has to be carried out only once, and is reused for all iterations and all time steps. It should also be pointed out that the method is fully parallelizable in the directions space.

The stability problem is due to the fact that accuracy increases with flatter RBFs (shape parameter $c \to \infty$). But then, the basis functions become approximately constant and the resulting system becomes ill-conditioned. Thus, there is a trade-off between accuracy and stability which requires a careful selection of the shape parameter. This selection is specially complex in the case of non-equispaced nodes, where the value of the shape parameter should be node dependent (usually a function of the distance to its nearest neighbour), and where we have observed that the numerical results are very sensitive to the values of the shape parameters.

Finally, it should be mentioned that, in order to address larger 2D or 3D problems with the RBF technique, domain decomposition methods with alternating directions algorithm [55] could be used to accelerate matrix factorization [6,45] and alleviate ill-conditioning.

Acknowledgments

This work has been supported by the Spanish MECD Grants MAT2005-05730 and FIS2007-62673 and by Madrid Autonomous Region Grant S-0505.

References

[1] G. Bal, M. Moscoso, Polarization effects of seismic waves on the basis of radiative transport theory, Geophys. J. Int. 142 (2000) 571–585.
[2] L.B. Barichello, C.E. Siewert, The searchlight problem for radiative transfer in a finite slab, J. Comput. Phys. 157 (2000) 707–726.
[3] R.K. Beatson, W.A. Light, S. Billings, Fast solution of the radial basis function interpolation equations: domain decomposition methods, SIAM J. Sci. Comput. 22 (2000) 1717–1740.
[4] J.B. Cherrie, R.K. Beatson, G .N. Newsam, Fast evaluation of radial basis functions: methods for generalized multiquadrics in $\mathbb{R}^n$, SIAM J. Sci. Comput. 23 (2002) 1549–1571.
[5] F. Bernal, M. Kindelan, RBF meshless modelling of non-Newtonian Hele–Shaw flow, Engng. Anal. Bound. Elem. 31 (2007) 863–874.
[6] F. Bernal, M. Kindelan, On the enriched RBF method for singular potential problems, Eng. Anal. Bound. Elem. 33 (2009) 1062–1073.
[7] K. Case, P. Zweifel, Linear Transport Theory, Addison-Wesley, Reading, MA, 1967.
[8] S. Chandrasekhar, Radiative Transfer, Dover, New York, 1960.
[9] L.M. Delves, J.L. Mohamed, Computational Methods for Integral Equations, Cambridge University Press, 1985.
[10] O. Dorn, A transport–backtransport method for optical tomography, Inv. Probl. 14 (1998) 1107–1130.
[11] T.A. Driscoll, B. Fornberg, Interpolation in the limit of increasingly flat radial basis functions, Comput. Math. Appl. 43 (2002) 413–422.
[12] G.E. Fasshauer, Newton iteration with multiquadrics for the solution of nonlinear PDEs, Comput. Math. Appl. 43 (2002) 423–438.
[13] G.E. Fasshauer, Meshfree Approximation Methods with MATLAB, World Scientific Publishing Co., Singapore, 2007.
[14] A.I. Fedoseyev, M.J. Friedman, E.J. Kansa, Improved multiquadric method for elliptic partial differential equations via PDE collocation on the Boundary, Comput. Math. Appl. 43 (2002) 439–455.
[15] A.J.M. Ferreira, P.A.L.S. Martins, C.M.C. Roque, Solving time-dependent engineering problems with multiquadrics, J. Sound Vib. 280 (2005) 595–610.
[16] A.J.M. Ferreira, C.M.C. Roque, R.M.N. Jorge, E.J. Kansa, Static deformations and vibration analysis of composite and sandwich plates using a layerwise theory and multiquadrics discretization, Eng. Anal. Bound. Elem. 29 (2005) 1104–1114.
[17] N. Flyer, G.B. Wright, Transport schemes on a sphere using radial basis functions, J. Comput. Phys. 226 (2007) 1059–1084.
[18] B. Fornberg, T.A. Driscoll, G. Wright, R. Charles, Observation of the behavior of radial basis function approximations near boundaries, Comput. Math. Appl. 43 (2002) 473–490.
[19] B. Fornberg, G.B. Wright, E. Larsson, Some observations regarding interpolants in the limit of flat radial basis functions, Comput. Math. Appl. 47 (2004) 37–55.
[20] B. Fornberg, G.B. Wright, Stable computation of multiquadric interpolants for all values of the shape parameter, Comput. Math. Appl. 48 (2004) 853–867.
[21] B. Fornberg, C. Piret, A stable algorithm for flat radial basis functions on a sphere, SIAM J. Sci. Comput. 30 (2007) 60–80.
[22] B. Fornberg, C. Piret, On choosing a radial basis function and a shape parameter when solving a convective PDE on a sphere, J. Comput. Phys. 227 (2008) 2758–2780.
[23] R. Franke, Scattered data interpolation: tests of some method, Math. Comput. 38 (1982) 181–200.
[24] H. Gao, H. Zhao, A fast forward solver of radiative transfer equation, Transport Theor. Stat. Phys. 38 (2009) 149–192.
[25] P. González-Rodríguez, A.D. Kim, Comparison of light scattering models for diffuse optical tomography, Opt. Express 17 (2009) 8756–8774.
[26] O. Guven, Y. Bayazitoglu, Radiative heat transfer solutions for anisotropically scattering media: the use of wavelets, J. Thermophys. Heat Transfer 18 (2) (2004) 172–177.
[27] R.L. Hardy, Multiquadric equations of topography and other irregular surfaces, J. Geophys. Res. 176 (1971) 1905–1915.
[28] L. Henyey, J. Greenstein, Diffuse radiation in the galaxy, Astrophys. J. 93 (1941) 70–83.
[29] Y.C. Hon, K.F. Cheung, X.Z. Mao, E.J. Kansa, A multiquadric solution for the shallow water equation, ASCE J. Hydraulic Eng. 125 (1999) 524–533.
[30] Y.C. Hon, M.W. Lu, W.M. Xue, Y.M. Zhu, Multiquadric method for the numerical solution of biphasic mixture model, Appl. Math. Comput. 88 (1997) 153–175.
[31] H.C. van de Hulst, Multiple Light Scattering, vols. 1 and 2, Academic Press, New York, 1980.
[32] E.J. Kansa, Multiquadrics, a scattered data approximation scheme with applications to computational fluid dynamics. I. Surface approximations and partial derivatives estimates, Comput. Math. Appl. 19 (1990) 127–145.
[33] E.J. Kansa, Multiquadrics, a scattered data approximation scheme with applications to computational fluid dynamics. II. Solutions to parabolic, hyperbolic and elliptic partial differential equations, Comput. Math. Appl. 19 (1990) 147–161.
[34] E.J. Kansa, Y.C. Hon, Circumventing the ill-conditioning problem with multiquadric radial basis functions: applications to elliptic partial differential equations, Comput. Math. Appl. 39 (2000) 123–137.
[35] A.D. Kim, A. Ishimaru, Chebyshev spectral method for radiative transfer equations applied to electromagnetic wave propagation and scattering in a discrete random medium, J. Comput. Phys. 152 (1999) 264–280.
[36] A.D. Kim, M. Moscoso, Chebyshev spectral methods for radiative transfer, SIAM J. Sci. Comput. 23 (2002) 2075–2095.
[37] A. D Kim, M. Moscoso, Radiative transport theory for optical molecular imaging, Inv. Probl. 22 (1) (2006) 23–42.

[38] V.B. Kisslelev, L. Roberti, G. Perona, An application of the finite-element method to the solution of the radiative transfer equation, J. Quant. Spectros. Radiat. Transfer 51 (1994) 603–614.
[39] A.D. Klose, V. Ntziachristos, A.H. Hielscher, The inverse source problem based on the radiative transfer equation in optical molecular imaging, J. Comput. Phys. 202 (2005) 323–345.
[40] E. Larsson, B. Fornberg, A numerical study of some radial basis function based solution methods for elliptic PDEs, Comput. Math. Appl. 46 (2003) 891–902.
[41] E. Larsson, B. Fornberg, Theoretical and computational aspects of multivariate interpolation with increasingly flat radial basis functions, Comput. Math. Appl. 49 (2005) 103–130.
[42] V.M.A. Leitao, A meshless method for Kirchoff plate bending problems, Int. J. Numer. Methods Eng. 52 (2001) 1107–1130.
[43] E.E. Lewis, W.F. Miller, Computational Methods of Neutron Transport, ANS Inc., La Grange Park, IL, 1993.
[44] E.E. Lewis, W.F. Miller Jr., Computational Methods of Neutron Transport, American Nuclear Society Inc., La Grange Park, IL, 1993.
[45] L. Ling, E.J. Kansa, Preconditioning for Radial Basis Functions with domain decomposition methods, Math. Comput. Model. 40 (2004) 1413–1427.
[46] W.R. Madych, S.A. Nelson, Multivariate interpolation and conditionally positive definite functions, Approx. Theory Appl. 4 (1988) 77–89.
[47] W.R. Madych, Miscellaneous error bounds for multiquadric and related interpolators, Comput. Math. Appl. 24 (12) (1992) 121–138.
[48] J. Moody, C.J. Daken, Fast learning in networks of locally-tuned processing units, Neural Comput. 1 (1989) 281–294.
[49] M. Moscoso, J. Keller, G. Papanicolaou, Depolarization and blurring of optical images by biological tissue, J. Opt. Soc. Am. A 18 (2001) 948–960.
[50] R. Platte, T.A. Driscoll, Computing eigenmodes of elliptic operators using radial basis functions, Comput. Math. Appl. 48 (2004) 561–576.
[51] B. Ritchie, P.G. Dykema, D. Braddy, Use of fast Fourier-transform computational methods in radiation transport, Phys. Rev. E 56 (2) (1997) 2217–2227.
[52] L. Ryzhik, G. Papanicolaou, J.B. Keller, Transport equations for elastic and other waves in random media, Wave Motion 24 (1996) 327–370.
[53] H. Sato, M.C. Fehler, Seismic Wave Propagation and Scattering in the Heterogeneous Earth, Springer-Verlag, New York, 1998.
[54] R. Schaback, Error estimates and condition numbers for radial basis function interpolation, Adv. Comput. Math. 3 (1995) 251–264.
[55] H.A. Schwarz, Gesammelte Mathematische Abhandlungen, Band 1, p. 11, Chelsea Publishing Co., Bronx, NY, 1972.
[56] P. Stott, A transport equation for the multiple scattering of electromagnetic waves by a turbulent plasma, J. Phys. A 1 (1968) 675–689.
[57] T. Tarvainen, M. Vauhkonen, V. Kolehmainen, J. Kaipio, Hybrid radiative-transfer-diffusion model for optical tomography, Appl. Opt. 44 (2005) 876–886.
[58] J. Tervo, P. Kolmonen, M. Vauhkonen, L.M. Heikkinen, J.P. Kaipio, A finite-element model of electron transport in radiation therapy and a related inverse problem, Inv. Probl. 15 (1999) 1345–1361.
[59] J.G . Wang, G.R. Liu, P. Lin, Numerical analysis of blot's consolidation process by radial point interpolation method, Int. J. Solids Struct. 39 (2002) 1557–1573.
[60] T.A. Wareing, J.M. McGhee, J.E. Morel, S.D. Pautz, Discontinuous finite element SN methods on three-dimensional unstructured grids, Nucl. Sci. Eng. 138 (3) (2001) 256–268.
[61] K. Watson, Multiple scattering of electromagnetic waves in an underdense plasma, J. Math Phys. 10 (1969) 688–702.
[62] Z. Wu, R. Shaback, Local error estimates for radial basis function interpolation of scaterred data, IMA J. Numer. Anal. 13 (1993) 13–27.
[63] Y. Zhang, K.R. Shao, Y.G. Guo, J.G. Zhu, D.X. Xie, J.D. Lavers JD, An improved multiquadric collocation method for 3-D electromagnetic problems, IEEE Trans. Magn. 43 (4) (2007) 1509–1512.